Evaluation of Synchrotron X-ray Computerized Microtomography for the Visualization of Dynamic Transport Processes in Low-porosity Materials

S.J. Altman,[1] M.L. Rivers,[2] W.J. Peplinski[1]
[1]Sandia National Laboratories, Albuquerque, NM, U.S.A.
[2]GeoSoilEnviro Consortium for Advanced Radiation Sources (GSECARS),
The University of Chicago, Chicago, IL, U.S.A.

Introduction

The purpose of this work is to evaluate synchrotron-source x-ray computerized microtomography (CMT) as a method for conducting visualization experiments to study dynamic processes. X-ray CMT is a nondestructive analytical technique that generates high-resolution, 3-D images of the transmission of x-rays through a material. Processes of interest for understanding solute transport include advection, diffusion, and sorption. An emphasis is on imaging pore space, where the dynamic process can be most readily visualized.

Visualization can be a powerful tool in studying processes that are normally studied by using bulk samples, such as column experiments [1, 2]. Visualization allows for determining which small-scale features in a sample control a process. Our focus is on low-porosity (<5%) geological materials; however, the results of this study can be extrapolated to higher-porosity samples and engineered materials. This work is more extensively described in Altman et al. [3].

Methods and Materials

Data were collected on two types of objects: (1) thick-walled capillary tubes, or resolution standards, with known pore-size diameters filled with 400 g of iodine (I) per liter (L) of potassium iodide (KI) solution, and (2) 5-mm-diameter rock cores saturated with 400 g I/L KI.

The resolution standards were used to determine (1) the minimum pore-space size that can be visualized and (2) the value for a cutoff linear absorption coefficient μ to differentiate pore space from solid sample. The pore space was filled with 400 gI/L KI. Data on the resolution standards were collected both above and below the absorption edge of I. A difference image was generated by subtracting the image taken below the x-ray absorption edge to that taken above the x-ray absorption edge. To remove some of the random noise in the image, a nine-point median smoothing routine was applied to the data. The method goes through the image slice by slice and assigns each voxel the median of that voxel and its eight surrounding voxels (a 3×3 square with the voxel in the center).

The KI-saturated geological samples were used to test whether CMT was effective at imaging pore space in geological samples (with an emphasis on low-porosity samples). Rock cores were vacuum saturated and the pressure saturated. Data were collected both above and below the absorption edge of I. Pore space in the geological samples was determined by first calculating a difference image. As occurred with the resolution standards, some random noise was removed from the image by applying a nine-point median smoothing routine. A cutoff linear absorption coefficient value of 2 cm^{-1} was used to differentiate pore space from solid material.

Results

When the resolution standards were imaged, the pore space of ≥51 μm in diameter could be readily visualized (Fig. 1). The 25 μm-diameter pore space was inconsistently detected. The 51- and 25-μm diameters correspond to diameters of approximately five and two voxels, respectively. Therefore, the resolution of this imaging process is somewhere around two voxels or greater. Note that these data were collected with the charge-coupled device (CCD) camera binning a

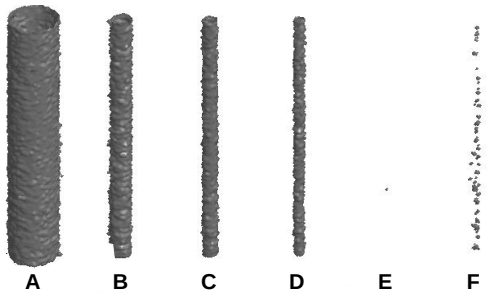

FIG. 1. Images of pore spaces with diameters of 254 μm (A), 102 μm (B), 76 μm (C), 51 μm (D), and 25 μm (E) with a cutoff value of 3 cm^{-1}, and of a 25 μm-diameter pore space with a cutoff value of 2 cm^{-1} (F). A length of approximate 1 mm for each tube is shown here.

2×2 square of pixels into one pixel. Thus, without the binning, the length of the side of a voxel could be one-half of what was obtained, or approximately 5 μm. If two to three voxels are needed to see the pore space, then the resolution becomes 10 to 15 μm.

Pore space could be detected in all of the geological samples (Fig. 2). Figure 2 presents a portion of different slices of the 3-D images of three different geological samples. An image of the samples taken below the iodine aborption edge (Fig. 2A1, 2B1, and 2C1), the raw difference image (Fig. 2A2, 2B2, and 2C2), and a pore-space visualization image using a cutoff linear absorption coefficient value of 2 cm^{-1} (Fig. 2A3, 2B3, and 2C3) are shown for each sample. The slices were chosen as representative slices or to make a specific point. Fig. 2A and 2B show slices perpendicular to the axis of the core. Fig. 2C presents slices parallel to the axis of the core. Images below the absorption edge are shown to determine whether or not pore space could be identified without the aide of the iodine tracer. Fig. 2B4 is a 3-D image using two different cutoff values to show the spatial relationship between a highly x-ray-absorbent mineral and pore space.

There are some clear differences between the different geological samples. The most pore space was visualized in the granodiorite. This observation is consistent with the higher porosity in the granodiorite core. Both the diorite and the shear-zone material had minimal pore space detected. The majority of the pore space in the diorite was detected at the end of the core and was thought to be due to sample preparation damage (Fig. 2C). The pore space in the granodiorite appears to be associated with the felsic minerals (lighter areas in Fig. 2A1) in the core. The pore space detected in the shear-zone material appears to be adjacent to a pyrite, magnetite, or other iron-rich mineral (Fig. 2B1 and 2B4). For this sample, the pore space shown in Fig. 2B was the only major pore space visualized in the section of the core.

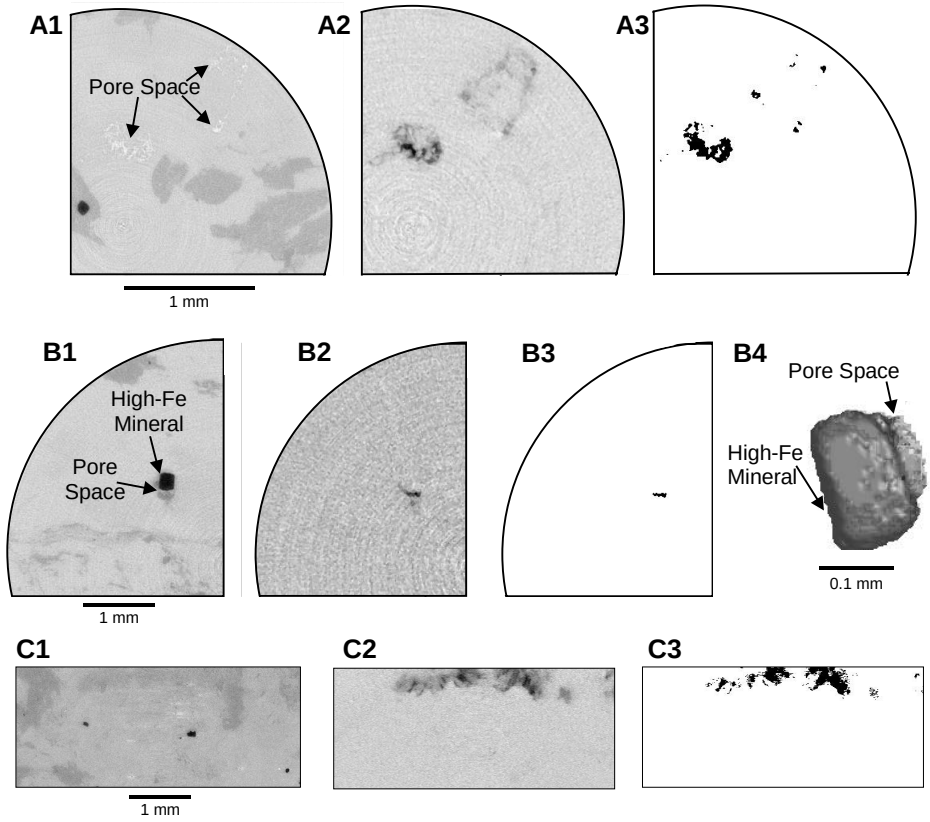

FIG. 2. Images of cores of granodiorite (A), shear-zone materials (B), and diorite (C). A1, B1, and C1 show linear absorption coefficient measurements collected at an energy just below the iodine absorption edge. Dark areas represent highly absorbent materials in these images. Lighter areas indicate pore space. A2, B2, and C2 show the raw differences in linear absorption coefficients collected at an energy just above and below the iodine absorption edge. Iodine in pore space is represented as dark areas. A3, B3, and C3 show processed data where difference values are above 2 cm^{-1} linear absorption coefficient. Dark areas represent pore space detected by CMT. B4 shows a 3-D enlargement of the iron-bearing mineral and associated pore space.

Several lines of evidence indicate that there is small-scale pore space in the rock cores that CMT is not capturing. These are discussed in more detail in Ref. 3.

Discussion

Absorption-edge differencing imaging (AEDI) with CMT is introduced as a method to enhance pore space imaging. We have demonstrated that we can clearly visualize a pore space that is 51 μm in diameter and inconsistently visualize a 25-μm pore space. Given the voxel size, this translates to a resolution of two or three voxels. With some alterations to data collection methods, discussed below, visualization of smaller pore space is possible.

Resolution can be measured in microns or voxels. The resolution of the system in microns is determined by the scintillator (the resolution of which is energy dependent), the optics, and the mechanical accuracy of the system. The resolution in voxels is determined by this system resolution and by voxel size. The voxel size, in turn, is dependent on the size of the sample (and therefore the amount it can be magnified) and the CCD camera.

The resolution in these experiments is limited by the larger sample size, the fact that we are binning the CCD camera data, and the fact that we are working at a high energy of 33-36 keV. With a smaller sample, we would be able to magnify the visible light image to a greater extent. In addition, not binning the CCD data would allow us to double the resolution. However, if we choose to use iodine to enhance the visualization of the pore space, we cannot decrease the x-ray energy. In addition, many geological samples require higher energy for sufficient x-ray transmission. Koch et al. [4] demonstrated submicron resolution and visualization of details down to 2 μm in size in tomographic images collected at 10 keV. So, under the right conditions, a pore space as small as 2 μm or less could be visualized. However, it would be difficult to get a resolution so fine by using AEDI and geological samples. For 1-cm-diameter samples, it is possible to collect voxels of 17 μm (binnned) and 8 μm (unbinned) on a side. With a 0.5-cm-diameter core and by using AEDI, we were able to minimize the voxel size to approximately 10 μm on a side; thus, unbinned data would lead to a voxel size of 5 μm on a side. Thus, the resolution could be 10 to 20 μm. To improve the effectiveness of AEDI, it is best to use as high a tracer concentration as possible. This is especially true for smaller pores.

Synchrotron-based x-ray imaging will work best on fine-grained geological or engineered materials. With larger-grained materials, it is difficult to define an appropriate representative elemental volume (REV) and have a sample of the appropriate size for imaging. The larger the sample, the larger the voxel size and the fewer the x-rays that will be transmitted through the sample. We imaged samples up to 1 cm in diameter successfully.

We originally stated that the purpose of this work was to evaluate CMT as a technique for visualizing dynamic processes, such as flow and transport. We have shown that CMT can be used to visualize both pore space and cesium (Cs) sorbed onto clay minerals. On the basis of this work, we have identified the following conditions that must exist for CMT to be effective. First, the process being studied must be slow enough that great changes do not occur within the approximately 25 to 50 minutes needed to collect the data. Because of advances in instrumentation, Wildenschild et al. [5] anticipate a significant reduction in the time required for a full scan at GSECARS. However, for 1/4-degree rotation increments and a 1-second x-ray exposure time, the minimum data collection time (assuming no delays due to data transmission, stage movement, and collection of white-field images) would be 12 minutes. Likewise, for a 1/2-degree exposure time, the ideal minimum data collection time would be 6 minutes. The larger the rotation angle increment, the greater the noise in the imaging process. Second, tracer can be detected only in areas greater than the resolutions discussed above. In the case of the crystalline rocks used here, the pore space controlling transport through the sample could not be visualized. However, in samples with larger pore space, tracer detection would be more likely. Unfortunately, the larger pore space could also mean that the processes will occur at a time scale faster than can be resolved by using CMT.

Acknowledgments

This project was funded by the U.S. Department of Energy (DOE) Waste Isolation Pilot Plant (WIPP) International Program and by the U.S. Nuclear Regulatory Commission (NRC). D. Bronowski is thanked for his help in core preparation. A. McLain helped to collect some of the data. We are grateful for the help of D. Lucero in the early stages of this project. D. Lenz of Research Systems, Inc., is thanked for her help in programming IDL to assist in the data processing. A. Winberg and SKB, M. Uchida and JNC, and P. Marschall and Nagra are thanked for supplying samples from the Äspö URL site, the Kamaishi mine, and the Grimsel test site, respectively. Sandia is a multiprogram laboratory operated by Sandia Corporation, a Lockheed Martin Company, for DOE under Contract No. DE-AC04-94AL85000. GSECARS is supported by the National Science Foundation (EAR-0217473), DOE Geosciences (DE-FG02-94ER14466), and the State of Illinois. Use of the APS was supported by the DOE Office of Science, Office of Basic Energy Sciences, under Contract No. W-31-109-ENG-38.

References

[1] S.J. Altman, M. Uchida, V.C. Tidwell, C.M. Boney, and B.P. Chambers, J. Contam. Hydrol. (in press, expected publication December 2003).

[2] V.C. Tidwell, L.C. Meigs, T. Christian-Frear, and C.M. Boney, J. Contam. Hydrol. **42**(2-4), 285-302 (2000).

[3] S.J. Altman, W.J. Peplinski, and M.L. Rivers, J. Contam. Hydrol. (in review, 2003).

[4] A. Koch, C. Raven, P. Spanne, and A. Snigirev, J. Opt. Soc. Am. A **15**(7), 1940-1951 (1998).

[5] D. Wildenschild, J. Hopmans, C. Vaz, M. Rivers, D. Rikard, and B. Christensen, J. Hydrol. **267**(3-4), 285-297 (2002).